



HAL
open science

Microstructural and mechanical properties of biocomposites made of native starch granules and wood fibers

Arnaud Regazzi, Maxime Teil, Pierre J.J. Dumont, Barthelemy Harthong, Didier Imbault, R. Peyroux, Jean-Luc Putaux

► To cite this version:

Arnaud Regazzi, Maxime Teil, Pierre J.J. Dumont, Barthelemy Harthong, Didier Imbault, et al. Microstructural and mechanical properties of biocomposites made of native starch granules and wood fibers. *Composites Science and Technology*, 2019, 182, pp.107755. 10.1016/j.compscitech.2019.107755 . hal-02199850

HAL Id: hal-02199850

<https://hal.univ-grenoble-alpes.fr/hal-02199850v1>

Submitted on 31 Jul 2019

HAL is a multi-disciplinary open access archive for the deposit and dissemination of scientific research documents, whether they are published or not. The documents may come from teaching and research institutions in France or abroad, or from public or private research centers.

L'archive ouverte pluridisciplinaire **HAL**, est destinée au dépôt et à la diffusion de documents scientifiques de niveau recherche, publiés ou non, émanant des établissements d'enseignement et de recherche français ou étrangers, des laboratoires publics ou privés.

Microstructural and mechanical properties of biocomposites made of native starch granules and wood fibers

Arnaud Regazzi^{a,b}, Maxime Teil^{a,b}, Pierre J.J. Dumont^{c,*}, Barthélémy Harthong^b, Didier Imbault^b, Robert Peyroux^b, Jean-Luc Putaux^d

^a Univ. Grenoble Alpes, CNRS, Grenoble INP, LGP2, F-38000, Grenoble, France

^b Univ. Grenoble Alpes, CNRS, Grenoble INP, 3SR, F-38000, Grenoble, France

^c Univ. Lyon, INSA-Lyon, LaMCoS CNRS UMR5259, F-69621, Lyon, France

^d Univ. Grenoble Alpes, CNRS, CERMAV, F-38000, Grenoble, France

ARTICLE INFO

Keywords:

- A. short-fiber composites
- B. Mechanical properties
- C. Multiscale modeling
- E. Powder processing

ABSTRACT

Novel biocomposites were fabricated using preforms of unmodified starch powder and wood pulp fibers. Stacks of preforms were consolidated using thermo-compression (TCM) and ultrasonic compression moldings (UCM). The characterization of the microstructure of the biocomposites showed that TCM enabled a better preservation of the crystallinity of starch granules during their welding than UCM. However, UCM allowed a significant gain in processing time. For the best set of forming and material parameters, the composites exhibited an elastoplastic response with strain hardening. Their Young's modulus, flexural strength and strain at ultimate stress reached up to approx. 6 GPa, 70 MPa, and 8%, respectively. The best properties were associated to the partial preservation of the native crystallinity of starch and lowered porosity. Bleached and fibrillated fibers with a large aspect ratio also contributed to the enhancement of composite properties. These effects were explained by a better starch-fiber interface and the presence of a network of connected fibers within the composites.

1. Introduction

The need for sustainable materials in the field of polymer-matrix composite materials prompted the growing use of biopolymer matrices and bio-based reinforcement fibers. Several bio-based components exhibit excellent native mechanical properties and are promising candidates as raw materials for biocomposites with enhanced mechanical properties. Plant and wood fibers (elastic modulus $5 < E < 90$ GPa), as well as unmodified starch granules (elastic modulus ≈ 3 GPa) exhibit interesting mechanical properties because of their nanoscale semi-crystalline structure [1–4]. Both materials are also interesting because their extraction chains are well established and their cost is relatively low. Starch-based composites have been widely investigated. Starch is usually plasticized, *i.e.* thermally-processed with water and other plasticizers, and blended with other polymeric materials [5]. It can be associated with various fiber reinforcements, including nano- and micrometric bio-based fibers [6–8]. Classical composite-forming processing routes such as extrusion and injection result in a complete modification of the structure of starch, inducing a possible recrystallization, and/or degradation [5,6]. The mechanical properties of injection-molded starch-based composites can range between 0.6 and 8.3 GPa for

the elastic modulus, 7.6 and 51 MPa for the tensile strength, depending on the fiber content and the amount of plasticizer when, for instance, starch acetate is associated with cellulosic fibers [9,10]. The use of native starch granules is less widely spread except as fillers in polymers to reinforce plastics [6]. Recently, unmodified starch granules have been used to obtain reinforced polymer matrices by taking advantage of starch-absorbed moisture to initiate polymerization or cross-linking reactions [11]. Starch granules have also been used to anchor and support graphene oxide (GO) nanosheets to enhance the dispersion of these nanoparticles in poly(lactic acid) PLA matrix [13]. This approach resulted in PLA/GO@starch composites with properties outperforming those of PLA/starch composites. Furthermore, the dielectric properties of starch granules can be used to control their dispersion in elastomeric matrices and obtain enhanced mechanical properties [12]. It was shown that unmodified starch granules could also be used to fabricate parts by compression molding without using chemical additives, while controlling the amount of absorbed water and preserving their native crystalline structure [3]. These materials exhibit Young's moduli that are comparable to those of usual thermoplastic matrices such as PVC, PS or PMMA. However, the presence of defects such as porosity or cracks, is detrimental to their strength properties.

* Corresponding author.

E-mail address: pierre.dumont@insa-lyon.fr (P.J.J. Dumont).

In this study, the manufacturing of biocomposites was investigated using thermo-compression molding (TCM) as a long-cycle technique [3] and ultrasonic compression molding (UCM) as a short-cycle technique [14] without adding any chemicals. In both techniques, starch granules were mixed with wood pulp fibers using a papermaking process to enhance both the elastic and strength properties of unmodified starch matrices. The objective was to evaluate both the microstructure and mechanical properties of the resulting bio-based composites, and to assess the suitability of both techniques for preserving the microstructural properties of the biocomposite constituents.

2. Experimental

2.1. Materials

2.1.1. Starch

Two different sources of starch granules were used, differing by both their amylopectin/amylose ratio and crystalline structure: (i) a waxy maize starch C*Gel 04201 from Cargill, that contained 99% of amylopectin and exhibited an A-type crystalline structure, and (ii) an amylo maize starch N-460 from Roquette with 50% of amylopectin and a B-type crystalline structure.

2.1.2. Pine wood fibers

Both a chemo-thermomechanical pulp (CTMP), *i.e.* rich in lignin, and a bleached chemical Kraft pulp (CB), *i.e.* where the lignin was extracted from fibers, were used. They were obtained from pine wood. The CB pulp was refined using a PFI mill (10,000 rotations). The de-watering properties of the pulp fibers were assessed using a Schopper-Riegler index testing device [15]. Besides, their morphology was evaluated using a fiber and shive analyzer MorFi from TechPap (Grenoble, France). The results are summarized in Table 1 and showed, as expected, that the CB pulp was much more fibrillated than the CTMP pulp.

2.2. Processing

2.2.1. Preform manufacturing

In order to disperse fibers into the starch powder matrix, semi-products were manufactured in the form of sheets. First, the appropriate amount of pulp was weighed. This amount depended on the targeted fiber content, such that the weight of the granules/fibers mix was 10 g for all sheets. Then, the pulp was immersed in 1 L of distilled water. The preparation was mixed for 5 min in a domestic blender to disperse fibers. Then, starch powder was added and slowly stirred with fibers for 20 min to obtain a homogeneous suspension. Preform sheets of 20 cm in diameter were obtained by filtering the suspension using a Rapid Köthen sheet former and a 1 μ m filter cloth. Then, sheets were oven-dried at 40 °C overnight and cut into layers matching the dimensions of the molds. Finally, the molds were filled with a stack of starch/fibers layers to achieve a given mass (constant for each technique). Fig. 1 shows SEM images of the cross sections of several preforms. These images reveal that for both types of fibers, starch granules were well trapped and intercalated within the fiber network during the filtering step of the preform manufacturing. However, a slight sedimentation of starch granules was also observed inside the preforms. In addition, these images show that fibers mainly exhibited a planar orientation due to the deposition process. Note the apparent fibrillation of fibers that is

much more pronounced for CB than CTMP pulp fibers, which agrees with the aforementioned results (Table 1). The fibrils of CB fibers coated the starch granules, showing a good affinity between both constituents. In addition, the lumens of the CTMP fibers were partially open, whereas those of CB pulp fibers were mostly closed. In these preforms, the pores were not only located inside and between the fibers, but also inside some starch granules that were hollow.

2.2.2. Thermo-compression molding (TCM) and ultrasonic compression molding (UCM)

TCM induces the welding of granules and fibers by conduction heating in quasi-static compression conditions. A processing temperature of 100 °C was applied to the thermo-regulated plates of the molding press while the compression stress was kept at 100 MPa for 60 min. Thermogravimetric analyses showed that this temperature was far below the degradation of starch and wood fibers (see also section 3.4). This compression stress was necessary to achieve a good cohesion in composites. Accounting for the amount of starch powder that ranged between 50 and 70 wt%, the relative part of compression stress on starch granules was roughly estimated to range between 30 and 70 MPa. These compression stresses were optimal to prepare starch-only samples with a good cohesion [3]. For this technique, a 80 \times 10 mm² stainless steel rectangular mold was designed. Eighteen or nineteen rectangular layers of semi-products were stacked into the mold cavity to reach a mass of 4.80 (\pm 0.05) g. After molding, samples with a thickness of approximately 4 mm were stored at least 12 h in a climate-controlled room at 23 °C and 50 % of relative humidity (R.H.) before characterization so as to reach an equilibrated moisture content.

The aim of UCM is to induce the welding of granules and fibers by local heating under the effect of viscous dissipation and/or inter-particle friction [16–18,35]. This technique consists in simultaneously applying a constant average compression stress of 15 MPa and a forced 20 kHz vibration of 60 μ m amplitude on the top of the sample during 0.70 s. During that time, the temperature of the sample should not increase over 200 °C, as measured by the authors during the ultrasonic welding of lignocellulosic materials [35]. Once again, this temperature was below the degradation temperatures of the constituents of the composite materials. For UCM, the mold was made of stainless steel and was a 32 \times 4 mm² oblong cavity. The filling technique was similar to that previously described for TCM, and the targeted material weight was 300 (\pm 15) mg, corresponding to a stacking of approximately 7 or 8 sheets. Again, after molding, samples with a thickness of about 1.6 mm were stored at least 12 h in a climate-controlled room at 23 °C and 50% R.H. before characterization so as to reach an equilibrated moisture content. UCM allows a significant gain in processing time compared to TCM. However, the effect of applying vibrations to starch-based composites maintained under compression is not known. This study thus allowed a comparison of the microstructure and mechanical properties of the materials prepared using both techniques.

2.3. Characterization methods

2.3.1. Density and bulk porosity measurements

The determination of the bulk density d_{bulk} of the samples was based on mass and volume measurements. The samples mass m was measured using a Mettler Toledo ME204 balance. Their thickness and width were assessed using a Mitutoyo Digimatic 293–821 μ m. Three measurements along the length of samples were used to define the mean value of these

Table 1
Morphological characteristics and Schopper-Riegler index of pine wood pulp fibers.

Pulp	Mean fiber length l [μ m]	Mean fiber width d [μ m]	Fibrillation index [%]	Fine content [% in area]	Schopper-Riegler index
CTMP	845	40.9	1.65	6.09	16
CB	1085	33.1	0.94	3.51	58

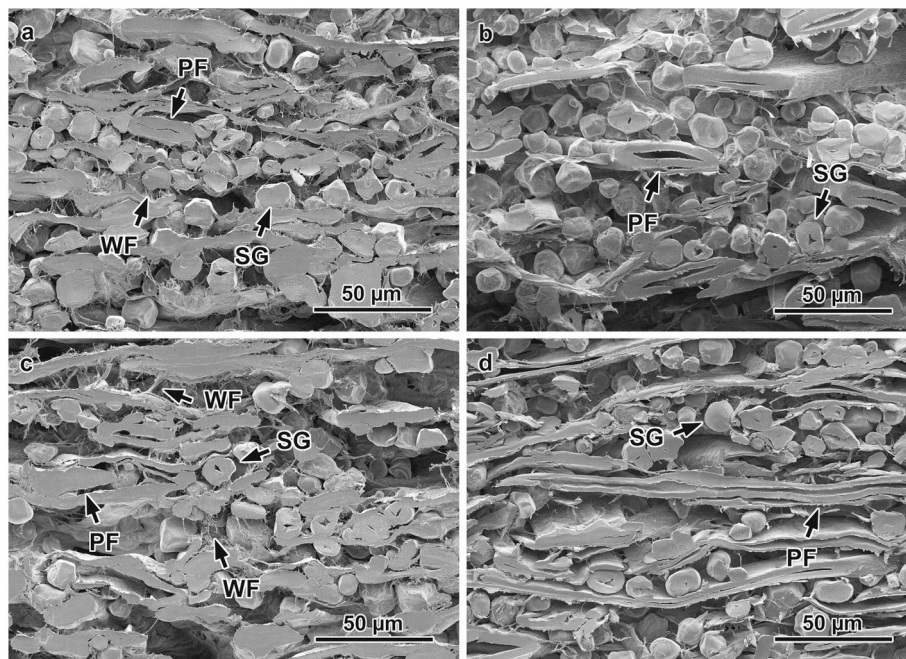


Fig. 1. SEM images of cross-sections of preforms made of softwood pulp and waxy maize starch granules: 30 wt% CB (a), 30 wt% CTMP (b), 50 wt% CB (c), 50 wt% CTMP (d). The arrows point at starch granules (SG), wood fibrils (WF) and pulp fibers (PF).

two dimensions. The length was measured using a Mitutoyo Absolute Digimatic 500-181 caliper. Finally, the volume V of samples was calculated using these measured dimensions making the assumption of a plane-parallel geometry. The density d_{bulk} is the ratio m/V . A helium pycnometer (Accupyc 1330, Micromeritics Instrument Corporation, USA) was used to measure the absolute density of starch granules d_{starch} and wood fibers d_{fiber} . The determination of volume was based on the reduction of the gas capacity of a chamber where the sample is placed. In practice, the device measures the pressure drop when the sample chamber is connected to an expansion chamber. All experiments were conducted in triplicate. The values of d_{starch} for waxy and amylo maize starches were 1.495 and 1.488, respectively. The values of d_{fiber} for CTMP and CB pulps were 1.486 and 1.542, respectively. The bulk porosity of composites Φ was evaluated from their bulk density d_{bulk} and absolute density d_{abs} , as follows:

$$\Phi = 1 - \frac{d_{bulk}}{d_{abs}}$$

where the absolute density of composites d_{abs} was determined from the absolute density of its constituents (d_{starch} and d_{fiber}) and the weight fiber content w , as follows:

$$d_{abs} = \frac{d_{starch} d_{fiber}}{w d_{starch} + (1 - w) d_{fiber}}$$

2.3.2. Thermogravimetric analysis (TGA)

The thermal stability of samples was evaluated by TGA (STA 6000, Perkin Elmer Instruments, USA), heating from 50 °C to 450 °C at a rate of 10 °C min⁻¹ under an air flow of 20 mL min⁻¹.

2.3.3. Bending tests

The mechanical properties of composites were determined by three-point bending tests. An Instron 5965 testing machine was used with a 5 kN force sensor. Considering the low stress levels, the deformation of the testing machine was neglected, and strain calculations were based on the crosshead displacement. Experiments were performed using a crosshead velocity of 2 mm min⁻¹ in accordance with the ISO178 standard. All experiments were conducted in triplicate in a climate-

controlled room at 23 °C and 50% R.H.

2.3.4. Scanning electron microscopy (SEM)

Preform samples were cut with a razor blade, coated with Au/Pd in a Baltech MED-020 sputter coater and the cross-sections were observed in secondary electron mode with a FEI Quanta-FEG 250 microscope operating at 1 kV. The processed composite samples were fractured in liquid nitrogen. The fracture surfaces were coated with Au/Pd in an Emitech K550X sputter coater and observed with a FEI Quanta 200 microscope operating at 10 kV.

2.3.5. X-ray diffraction (XRD)

The XRD analysis was conducted on starch only. Native starch granules and compacted starch materials ground to a fine powder were poured into glass capillaries of 1.5 mm outer diameter. The capillaries were flame-sealed and exposed to X-rays in a vacuum chamber using a Philips PW3830 generator operating at 30 kV and 20 mA (Ni-filtered CuK α radiation, $\lambda = 0.1542$ nm). Two-dimensional diffraction patterns were recorded on Fujifilm imaging plates. The plates were read off-line using a Fujifilm BAS 1800-II bio-imaging analyzer. The resulting ring patterns were radially averaged in order to get diffraction profiles.

2.3.6. X-ray microtomography

X-ray microtomography imaging experiments were performed at the European Synchrotron Radiation Facility (ESRF, ID19 beamline, Grenoble, France) to record 3D images of the microstructure of the central region of the samples (X-ray energy = 19 keV, CCD detector of 2560 × 2560 pixels, voxel size 0.324 μ m × 0.324 μ m × 0.324 μ m, scanning time < 5 min). The samples were placed vertically and their length was always orthogonal to the X-ray beam during scanning. The scans were reconstructed using the so-called Paganin procedure, which is based on the use of the phase contrast in the images [19,20]. Then, the ImageJ software was used to get binary images and filter noise [21]. Binarization was applied to extract either the fibrous network or the pores from the starch matrix. This segmentation was achieved by applying a threshold on the intensity of voxels. The volume fiber content and the porosity were defined as the ratio of the number of voxels corresponding to the volume of fibers and pores, respectively, over the

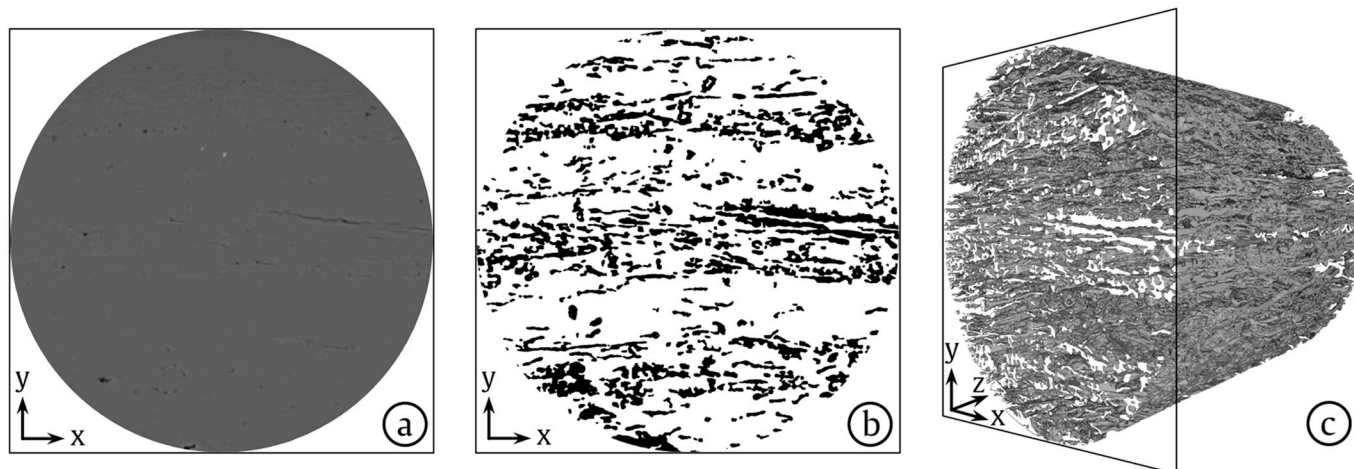


Fig. 2. Slices of X-ray microtomography images before (a) and after (b) binarization of fibers (pictures represent a square of 750 μm side length) – 3D image after binarization (c).

total number of voxels in the scanned volume. Typical images before and after treatment for the extraction of fibers are shown in Fig. 2. The volume of the 3D images was a 750 μm wide and 700 μm high cylinder. Only the CB/waxy maize starch composite obtained by UCM was used for the analysis of the volume fiber content, due to the difficulty of separating matrix and fibers when their density was close, resulting in a very low contrast between both phases.

3. Results

3.1. Visual aspects and handling of samples

The visual aspect of the different materials mainly depended on the nature of the reinforcement (Fig. 3). CB-reinforced composites were completely white, while CTMP-reinforced composites were light-brown due to the presence of lignin in CTMP fibers. For both processing techniques, the aspect of both sides of the samples was slightly different. The side in contact with the punch was slightly brighter than the opposite side (bottom of the mold), probably because of a denser and smoother surface. As a result, the visual aspect of the samples appeared to be controlled by the nature of the reinforcement as well as compaction heterogeneities [3].

3.2. Evolution of the crystallinity of starch

The crystallinity of waxy maize starch samples was assessed by XRD before and after forming. In order to avoid undesired diffraction peaks originating from fiber constituents, starch samples were fabricated in the same conditions than composite samples, except that the molds were directly filled with 100 wt% starch powder before processing. Starch samples had the same mass as composite samples, i.e. 4.8 g for TCM and 0.3 g for UCM. Fig. 4 shows the XRD profiles of as-received

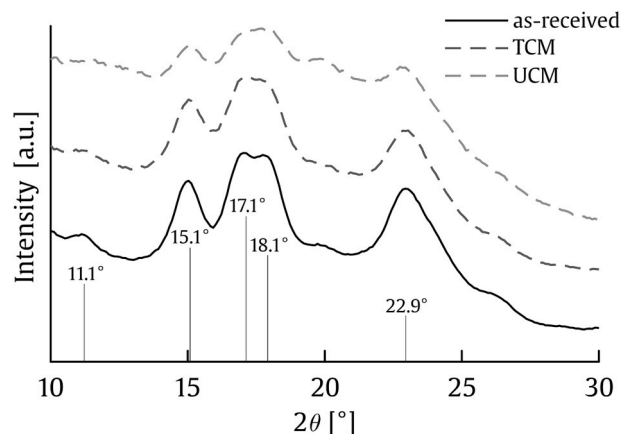


Fig. 4. XRD profiles of waxy maize starch samples before and after TCM and UCM. The profiles were shifted vertically for clarity.

starch, after TCM or UCM. The diffraction profile of the as-received starch exhibited diffraction peaks typical of the A-type allomorph, with the main peaks located at about 15.1°, 17.1°, 18.1°, and 22.9° diffraction angles [22]. The same diffraction peaks were observed for starch processed by TCM, with a slightly lower amplitude and a simultaneous increase of the amorphous background, indicating a slight decrease in the overall crystallinity of TCM-processed starch. A much more pronounced decrease of the peak intensity was observed for UCM-processed starch. Yet the diffraction peaks remained visible, indicating that UCM-processed starch was not amorphous. As a result, both TCM and UCM forming techniques produced cohesive samples (i.e. the welding of starch granules was successfully obtained) without completely modifying their crystalline structure (i.e. without completely decrystallizing

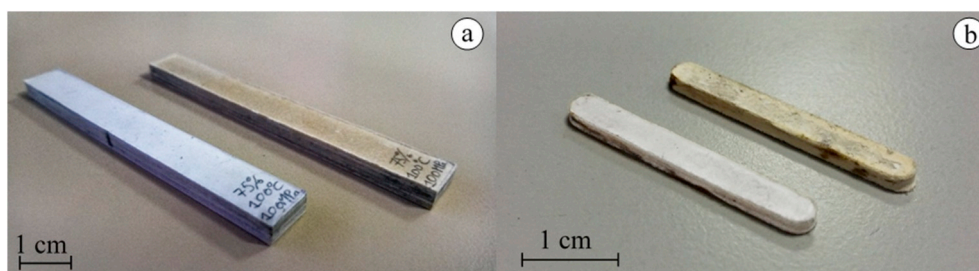


Fig. 3. CB/waxy (foreground) and CTMP/waxy (background) maize starch composites obtained by TCM (a) and UCM (b).

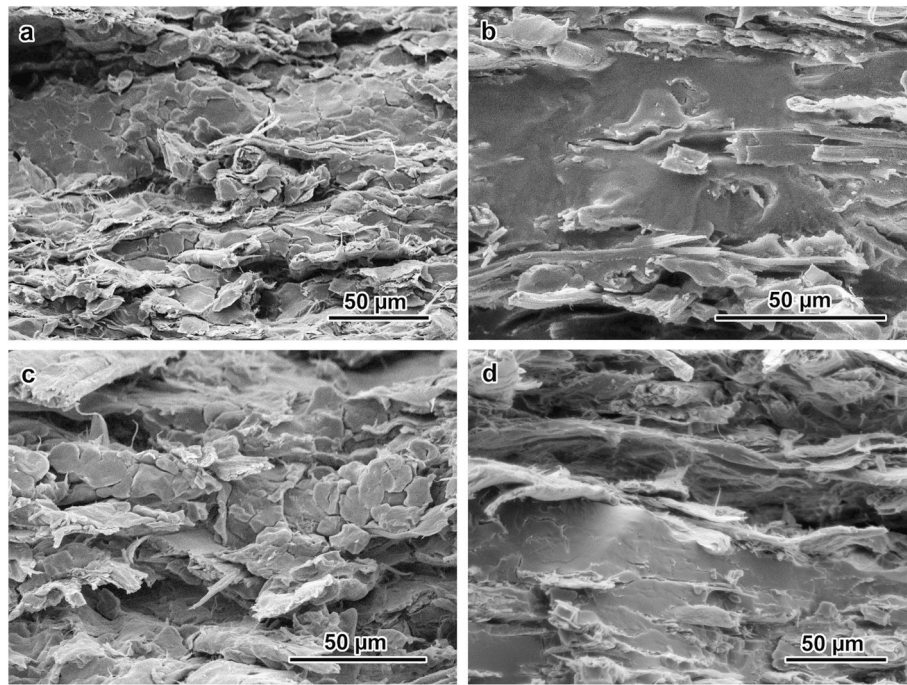


Fig. 5. SEM images of cryo-fracture surfaces of 50 wt%/50 wt% softwood pulp/waxy maize starch composites: a) TCM - CTMP, b) UCM - CTMP, c) TCM - CB, d) UCM - CB.

them). UCM induced a higher decrease in crystallinity of the starch granules compared to TCM. Assuming that the behavior of starch during processing was similar in the presence of fibers, both techniques enabled starch granules to be welded, while partially preserving their native crystallinity, and presumably their excellent mechanical properties. Investigating the crystallinity of both phases of the composite samples would be necessary to confirm this assumption. However, this would require using advanced XRD techniques for the deconvolution of the diffractograms of both starch and wood fibers.

The SEM images of fracture surfaces of cryo-fractured samples shown in Fig. 5 confirms that both processing techniques induced a rather different evolution of the powder-like starch matrix. A clear difference between the starch matrices obtained by TCM or UCM was observed. For TCM, the starch granules were extremely deformed and compressed, but still clearly visible (Fig. 5a,c), whereas, for UCM, the starch matrix was much more homogeneous, and the boundaries between the starch granules were hardly visible, confirming a drastic evolution of starch for this forming process.

3.3. Microstructure

Porosity – Table 2 gives the evolution of the bulk porosity of composites as a function of the weight fiber content for both molding techniques. The bulk porosity of TCM-processed samples was globally lower than that of UCM-processed samples. This difference was attributed to the difference in the compression stress: 100 MPa for TCM and 15 MPa for UCM. For both forming techniques, the bulk porosity also slightly increased with the fiber content, suggesting that pores were partially located close to fibers. For a given type of starch matrix, samples containing CTMP fibers showed a higher bulk porosity than samples containing CB fibers. This increase in porosity could be attributed to the usually higher stiffness of CTMP fibers that contained lignin compared to CB fibers [23]. This effect could also be enhanced by the refining treatment of CB fibers that might have decreased their stiffness [24].

The analysis of the X-ray microtomography 3D images gave quantitative data on the spatial distribution of fibers and the porosity at the core of samples (called the core porosity thereafter). The results given in Table 3 show that the mean core porosity of all specimens remained

Table 2
Bulk porosity and mechanical properties of pulp/starch composites.

Process	TCM				UCM			
	CB		CTMP		CB		CTMP	
Starch	waxy	amylo	waxy	amylo	waxy	amylo	waxy	amylo
Fiber content of 30 %								
Bulk porosity [%]	4.56 ± 0.75	7.50 ± 0.36	5.98 ± 0.09	9.17 ± 1.06	14.2 ± 0.23	14.7 ± 2.03	18.6 ± 0.17	16.8 ± 0.86
Young's Modulus [GPa]	5.30 ± 0.07	5.67 ± 0.22	4.79 ± 0.31	4.17 ± 0.09	4.31 ± 0.40	4.71 ± 0.23	4.76 ± 0.08	3.83 ± 0.02
Ultimate stress [MPa]	58.2 ± 3.0	69.3 ± 6.0	39.9 ± 3.1	25.9 ± 7.5	68.4 ± 3.9	63.3 ± 7.5	63.2 ± 2.2	50.4 ± 0.9
Strain at ultimate stress [%]	6.28 ± 0.55	4.33 ± 0.39	1.41 ± 0.12	1.41 ± 0.78	4.77 ± 0.20	3.64 ± 1.05	2.38 ± 0.20	2.69 ± 0.23
Fiber content of 50%								
Bulk porosity [%]	5.48 ± 0.37	8.82 ± 0.65	7.01 ± 0.96	11.16 ± 0.20	15.0 ± 1.25	17.6 ± 3.77	21.09 ± 1.70	19.8 ± 1.99
Young's Modulus [GPa]	5.38 ± 0.23	6.06 ± 0.69	5.24 ± 0.58	5.08 ± 0.20	5.17 ± 0.38	5.64 ± 0.50	5.76 ± 0.53	3.81 ± 0.25
Ultimate stress [MPa]	60.7 ± 3.3	70.8 ± 7.2	46.4 ± 5.7	34.4 ± 7.0	66.6 ± 9.4	66.8 ± 10.2	60.6 ± 8.5	53.3 ± 1.9
Strain at ultimate stress [%]	7.66 ± 0.34	4.54 ± 1.80	1.50 ± 0.12	0.85 ± 0.28	4.39 ± 0.93	3.31 ± 1.45	2.24 ± 0.47	2.53 ± 0.21

Table 3
Mean core porosity of pulp/starch composites fabricated by TCM and UCM.

Matrix	TCM		UCM	
	Waxy maize	Amylomaize	Waxy maize	Amylomaize
CTMP	3.0%	4.0%	2.6%	1.0%
CB	1.0%	2.1%	0.6%	1.5%

below 2%, regardless of the fiber content and the forming technique. However, the mean core porosity was lower than the bulk porosity given in Table 2. Two reasons could explain this difference. First, the volume analyzed by microtomography represented only a fraction of the volume of the sample. It means that the image analysis results could not be representative of the entire sample and it would be difficult to capture possible heterogeneities of the porosity of samples throughout its entire thickness. Second, errors could also originate from the dimensions of samples that were measured and used to calculate the bulk density, assuming perfectly planar faces. Such errors could be significant for small samples such as those made by UCM. Despite these differences, the results given in Table 3 confirm the trends that were seen from Table 2 regarding the role of the type of fibers and the nature of starch on the porosity. The results from 3D image analysis presented in Fig. 6a also revealed that the pores were predominantly located within the regions of high fiber density between the fibers. The concentration of pores in the vicinity of fibers most probably induced a weakening of the apparent fiber-fiber contact zones. This might explain why the fracture surfaces in Fig. 5 exhibit some fibers that were pulled out from the composites during breaking. Through-thickness porosity profiles were extracted from the 3D X-ray microtomography images, as shown for instance in Fig. 6b for the specimen from Fig. 6a. It reveals a non-uniform distribution of porosity through the thickness in the imaged volume of this specimen. This non-uniform distribution is certainly related to the change from one compacted preform to another. The less porous regions corresponded to the transition zones between the various stacked layers.

At a larger scale of analysis, it was also observed that the microstructure of samples fabricated by UCM depended on the distance from the horn of the ultrasonic machine. Basically, the welding of starch and fibers was improved in the vicinity of the horn. It was visible with the naked eye that the most porous zones were located at the bottom of the mold, opposite from the horn, where the attenuation of acoustic waves was maximum.

Fiber content - X-ray microtomography images also allowed studying the volume fiber content profile. For instance, a mean fiber volume content of 25 vol% was determined from Fig. 6b while the targeted weight content was 30 wt%, i.e. 29.4 vol%. This difference was attributed to the low contrast between the fibers and the starch matrix in the X-ray images because both materials had a very similar density. As a result, the measured volume fiber content was very sensitive to the threshold value used for segmenting fibers. Despite this difficulty to

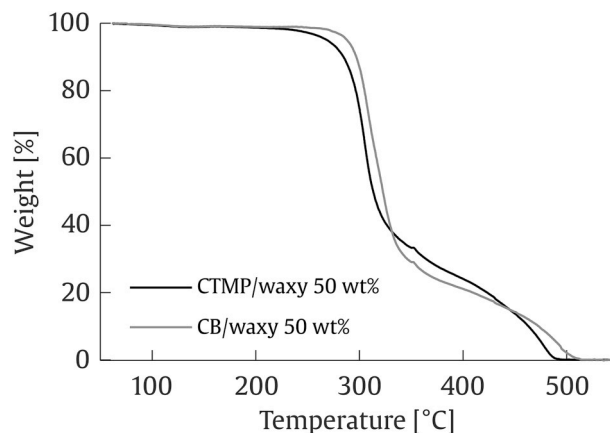


Fig. 7. Typical TGA curves obtained for TCM specimens made of waxy maize starch and CTMP fibers or CB fibers.

quantitatively assess the volume fiber content using X-ray microtomography, its variations revealed by this profile were significant and were again presumably related to the layered structure of the composite materials. In addition, as previously mentioned, preforms also exhibited a through-thickness heterogeneity. Such variations are commonly encountered for various types of industrial composite materials that are obtained by stacking several layers of preforms. For instance, parts that are fabricated using stacks of pre-impregnated short-fiber composites such as Sheet Molding Compounds (SMC) also exhibit this kind of through-thickness variations if their in-plane flow is limited [25].

3.4. Thermal behavior

Typical examples of TGA measurements are shown in Fig. 7 for starch/CB and starch/CTMP composites obtained using TCM. These curves reveal a 2 % weight loss from 50 to 150 °C attributed to the vaporization of water as temperature increased. Besides the degradation onset temperatures of both composites ranged between 220 and 240 °C, thus far above the temperatures reached during TCM or UCM.

3.5. Mechanical properties

Fig. 8a shows typical stress-strain curves obtained from bending experiments for two composites that were fabricated by TCM. Similar curves were obtained for composites fabricated by UCM. These curves typically show one initial quasi-linear sharp increase up to a transition stress above which the composites exhibit a more or less pronounced plastic regime with strain hardening up to a maximum stress, and then a slight decrease up to the sample breakage. Table 2 shows the Young's moduli of composites, the ultimate stress, i.e. the strength, defined as the maximum stress reached during bending tests, and the strain at the ultimate stress as a function of fiber content, for both processing

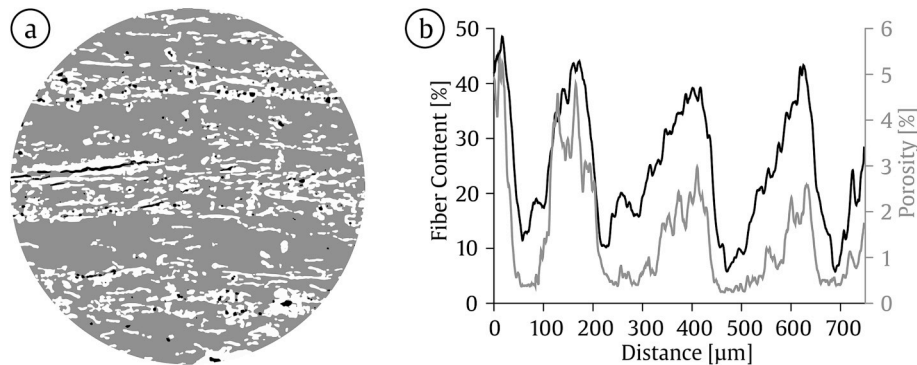


Fig. 6. (a) Slice of an X-ray microtomography image after segmentation of fibers (white), pores (black) and starch matrix (gray). The picture represents a 750-μm diameter circle for a sample of CB/waxy maize starch composite obtained by UCM. (b) Average fiber volume content (black curve) and core porosity (gray curve) along the thickness direction (y-axis of Fig. 2) of the same composite.

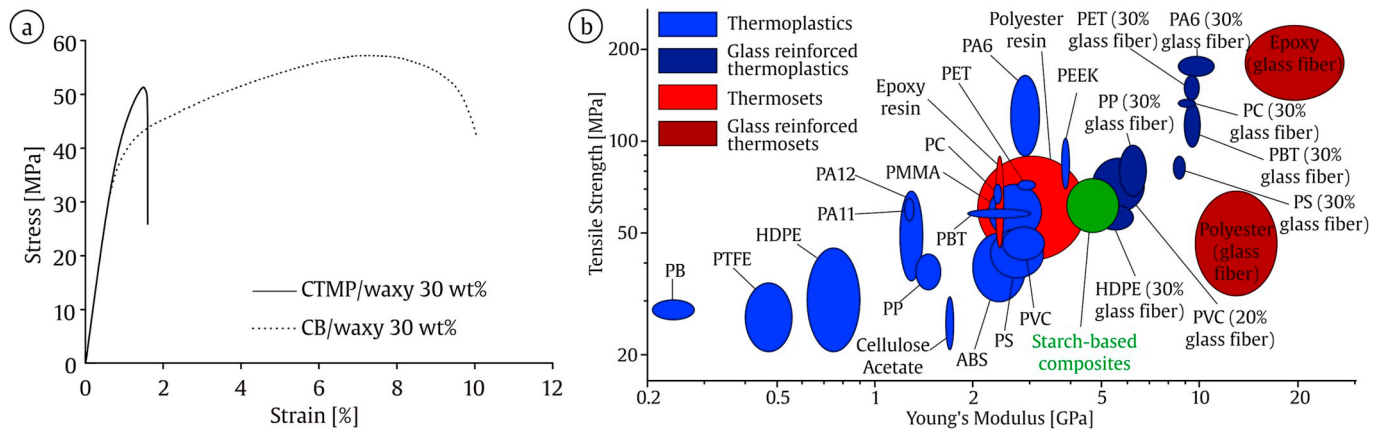


Fig. 8. (a) Typical stress-strain curves obtained from the bending tests of TCM specimens. (b) Tensile strength as a function of Young's modulus for the starch-based biocomposites and for some commercially-available polymers and composite materials.

techniques. For TCM (resp. UCM), the Young's moduli ranged between 4 and 6 GPa (resp. 3.8 and 5.6 GPa), whereas the strength ranged between 26.5 and 71 MPa (resp. 50 and 69 MPa), and the strain of samples at ultimate stress ranged from 0.9 to 7.6% (resp. 2.2 and 4.8%), showing an effect of the process conditions on the ultimate properties of biocomposites. Both strength and strain at ultimate stress depended more on the nature of the composite constituents for TCM than for UCM. The Young's modulus and the strength exhibited the same trend when the composite constituents varied. Indeed, for CB fibers, these mechanical properties were better with amylo maize starch matrix, whereas for CTMP fibers, they were better with waxy starch matrix. In addition, for both processing techniques, CB fibers induced an increase in the strain at ultimate stress compared with CTMP fibers.

4. Discussion

Role of fiber connectivity – In a previous study [3], the authors have shown that specimens made of pure waxy maize starch exhibited a maximum average Young's modulus of approximately 3 GPa, and average ultimate stress and strain that did not exceed 12 MPa and 0.4%, respectively, for the best set of TCM conditions. Further, the properties of specimens made of pure starch matrix that were fabricated using UCM exhibited similar properties (results not shown). Both starch matrices could be considered as particularly brittle. By comparison, adding fibers enhanced the elastic properties and the ultimate stress of starch matrices. In addition, the strain at ultimate stress of all studied composites was also greatly enhanced compared to that of the starch matrix alone. These results prove the leading role of the fibers in the composites obtained using both forming techniques. For the investigated fiber contents, the number of fiber-fiber contacts per fiber Z was roughly estimated using the statistical tube model [26–28]:

$$Z = 4\varphi_f \left(\frac{2}{\pi} r\varphi_1 + \varphi_2 + 1 \right)$$

where $r = l/d$ is the fiber aspect ratio, φ_f the fiber volume fraction, and φ_1, φ_2 orientation distribution functions ($\varphi_1 = \varphi_2 = 2/\pi$ for 2D planar random fibrous networks). Considering that $r = 21$ and 33 for CTMP and CB fibers, respectively (cf. Table 1), the number Z was estimated to range between 12 and 20 for CTMP fibers, and between 18 and 30 for CB fibers. This is in accordance with previous results for the number of contacts in paper fibrous networks [28]. Therefore, the presence of a network of fibers within the composites certainly plays a crucial role on the increase in their ultimate strain. It could also explain the yielding phenomenon in the plastic regime as such behavior is typically observed for papers [29]. Moreover, it can be assumed that after the matrix cracking, which is likely to occur for low strain ($\approx 0.4\%$), the strength of composites is controlled by the strength of the fiber

network.

Role of processing conditions – The Young's moduli were almost systematically higher when samples were fabricated by TCM instead of UCM. This effect could be interpreted as a consequence of the lower bulk porosity of TCM composites (section 5.3 and Table 2), but also from the lower starch crystallinity of the UCM composites.

Effect of constituents – Composites reinforced with CTMP fibers exhibited lower Young's moduli, ultimate stresses and strains than composites made of CB fibers. These trends can presumably be attributed to several origins: (i) the higher bulk and core porosities of CTMP reinforced composites (Tables 2 and 3), (ii) the smaller aspect ratio of CTMP fibers (Table 1), which limits the connectivity of the fiber network, and (iii) the starch-fiber interfacial properties. For the latter argument, fibrillation and the associated increased specific surface area of fibers could partially explain the better properties of CB fiber composites (see also Fig. 1). The physico-chemical properties of the interface are also important, as the properties of composites reinforced with CB fibers were better when made of amylo maize starch instead of waxy maize starch. It can also be noted that these starch-based composites exhibit comparable Young's moduli and ultimate stresses than those made of starch acetate and lignocellulosic fibers [9,10] or cellulose powders [30].

Potential mechanical properties of composites – The potential Young's modulus E of the CB fiber composites was estimated using the Halpin-Tsai-Kardos (HTK) model, assuming a 2D planar orientation of the fibers [31]:

$$E_{HTK} = 0.375E_L + 0.625E_T$$

$$\text{with } E_L = \frac{1 + 2(l/d)\eta_L\varphi_f}{1 - \eta_L\varphi_f} E_m \text{ and } E_T = \frac{1 + 2\eta_T\varphi_f}{1 - \eta_T\varphi_f} E_m \text{ where } \eta_L = \frac{E_f - E_m}{E_f + 2(l/d)E_m}$$

$$\text{and } \eta_T = \frac{E_f - E_m}{E_f + 2E_m}$$

The Young's modulus E_m of the starch matrix was considered to be 3 GPa [3], while the Young's modulus E_f of CB pulp fibers was reasonably chosen to range between 10 and 20 GPa [32]. In addition, the aspect ratio l/d of fibers involved in the HTK model was 33 (Table 1). The Young's modulus of these composites was also estimated using the extended Cox's model for planar fibrous structures with random orientations [27,33]:

$$E_{Cox} = 1/3\varphi_f E_f + (1 - \varphi_f)E_m$$

For $\varphi_f = 30\%$ and the HTK model, the Young's modulus of the CB fiber composites ranged between 4.6 GPa and 6.2 GPa, whereas for the Cox model, the Young's modulus ranged between 3.1 GPa and 4.1 GPa. For TCM and $\varphi_f = 30\%$, the actual Young's moduli of the composites (Table 2) were slightly higher than the theoretical predictions of Cox's model and in the same order of magnitude as the HTK model, e.g. 5.7 GPa and 5.3 GPa for CB fiber composites with amylo maize and

waxy maize starch, respectively. Since the experimental Young's moduli are close to the theoretical predictions, these results indicate (i) that there are good fiber-matrix interfacial properties of the composites, and (ii) the potential beneficial effect of the fiber-fiber contacts (which are not taken into account neither in the mean-field HTK model nor in Cox's model). For CB-fiber composites processed by UCM, both theoretical predictions and experiments are close, showing also good interfacial properties. However, at $\phi_f = 50\%$, the Young's moduli of composites seem to be lowered, possibly because of the increase in the number of fiber-fiber contacts with low interfacial properties or lowered fiber-matrix interfacial properties.

Comparison with polymers and other composite materials – Fig. 8b shows the mechanical performance of the obtained starch-based composites (green ellipse) in an Ashby-type materials selection chart [34]. The obtained composites exhibit interesting mechanical properties compared to various thermoplastic polymers such as high density polyethylene (HDPE), polypropylene (PP) or polyvinyl chloride (PVC) reinforced with glass fibers. Besides, the obtained composites exhibit mechanical properties that are comparable with the best properties of biocomposites using starch acetate as a matrix [9,10].

5. Conclusion

Bio-based composites were successfully prepared using a matrix made of waxy maize or amylo maize native starch granules, and softwood thermomechanical (CTMP) or bleached and fibrillated chemical Kraft (CB) pulp fibers. The specimens were processed using either thermo-compression (TCM) or ultrasonic compression (UCM) moldings of stacks of several preforms obtained by a papermaking-like technique. Both forming techniques produced composite samples with a good cohesion. XRD profiles showed that the native crystallinity of starch was better preserved in the case of TCM than UCM. SEM and X-ray microtomography images revealed the planar orientation of fibers within the preforms and the resulting biocomposites. Residual pores were mainly located between fibers, and more particularly in the regions with the highest fiber contents. These biocomposites exhibited an elastoplastic mechanical response. The partial preservation of the native crystallinity of starch, the lower porosity, the use of bleached and fibrillated fibers with a high aspect ratio contributed to enhance their mechanical performances. These effects were related to the presence of fiber-fiber contacts within the composites and improved starch-fiber interface properties. The mechanical properties of the biocomposites are comparable to those of other biocomposites made for instance of lignocellulosic fibers and starch acetate [9,10]. UCM does not provide as good properties as TCM. However, UCM is a fast (processing time of ca 1 s, resp. 1 h, for UCM, resp. for TCM) and energy-efficient solution to obtain the biocomposites. Further investigations are needed to better understand the influence of the type of starch and the source of pulp fibers on the properties of these new biocomposites.

Acknowledgments

The authors acknowledge the financial support of Institut Carnot PolyNat (Investissements d'Avenir - grant agreement #ANR-11-CARN-007-01), the NanoBio-ICMG Platform (FR 2607) for granting access to the electron microscopy facility, as well as Cécile Sillard and Raphaël Passas for their technical support, Bertine Khelifi (LGP2) and Christine Lancelon-Pin (CERMAV) for electron microscopy, and Romain Léger (C2MA) for pycnometer experiments.

References

- J. Schroeter, M. Hobelsberger, On the mechanical properties of native starch granules, *Starch* 44 (2006) 247–252, <https://doi.org/10.1002/star.19920440703>.
- D. Lourdin, J.-L. Putaux, G. Potocki-Véronèse, C. Chevigny, A. Rolland-Sabaté, A. Buléon, Y. Nakamura Y (Ed.), *Crystalline Structure in Starch*, Starch, Springer, Tokyo, 2015, pp. 61–90, https://doi.org/10.1007/978-4-431-55495-0_3.
- A. Regazzi, P.J.J. Dumont, B. Harthong, D. Imbault, R. Peyroux, J.-L. Putaux, Effectiveness of thermo-compression for manufacturing native starch bulk materials, *J. Mater. Sci.* 51 (2016) 5146–5159, <https://doi.org/10.1007/s10853-016-9817-7>.
- M.P.M. Dicker, P.F. Duckworth, A.B. Baker, G. Francois, M.K. Hazzard, P.M. Weaver, Green composites: a review of material attributes and complementary applications, *Compos. Part A* 56 (2014) 280–289, <https://doi.org/10.1016/j.compositesa.2013.10.014>.
- F. Xie, P.J. Halley, L. Avérous, Rheology to understand and optimize processibility, structures and properties of starch polymeric materials, *Prog. Polym. Sci.* 37 (2012) 595–623, <https://doi.org/10.1016/j.progpolymsci.2011.07.002>.
- L. Avérous, P.J. Halley, Biocomposites based on plasticized starch, *Biofuels*, *Bioprod. Biorefining* 3 (2009) 329–343, <https://doi.org/10.1002/bbb.135>.
- F. Xie, E. Pollet, P.J. Halley, L. Avérous, Starch-based nano-biocomposites, *Prog. Polym. Sci.* 38 (2013) 1590–1628, <https://doi.org/10.1016/j.progpolymsci.2013.05.002>.
- I.M.G. Martins, S.P. Magina, L. Oliveira, C.S.R. Freire, A.J.D. Silvestre, C.P. Neto, A. Gandini, New biocomposites based on thermoplastic starch and bacterial cellulose, *Compos. Sci. Technol.* 69 (2009) 2163–2168, <https://doi.org/10.1016/j.compscitech.2009.05.012>.
- K. Nättinen, S. Hyvärinen, R. Joffe, L. Wallström, B. Madsen, Naturally compatible: starch acetate/cellulosic fiber composites. I. Processing and properties, *Polym. Compos.* 31 (2010) 524–535, <https://doi.org/10.1002/pc.20833>.
- B. Madsen, R. Joffe, H. Peltola, K. Nättinen, Short cellulosic fiber/starch acetate composites – micromechanical modeling of Young's modulus, *J. Compos. Mater.* 45 (2011) 2119–2131, <https://doi.org/10.1177/0021998311401063>.
- L. Ceseracciu, J.A. Heredia-Guerrero, S. Dante, A. Athanassiou, I.S. Bayer, Robust and biodegradable elastomers based on corn starch and polydimethylsiloxane (PDMS), *ACS Appl. Mater. Interfaces* 7 (2015) 3742–3753, <https://doi.org/10.1021/am508515z>.
- L. Hao, Z. Shi, X. Zhao, Mechanical behavior of starch/silicone rubber hybrid electric elastomer, *React. Funct. Polym.* 69 (2009) 165–169, <https://doi.org/10.1016/j.reactfunctpolym.2008.12.014>.
- H. Xu, L. Xie, D. Wu, M. Hakkarainen, Immobilized graphene oxide nanosheets as thin but strong nanointerfaces in biocomposites, *ACS Sustain. Chem. Eng.* 4 (4) (2016) 2211–2222, <https://doi.org/10.1021/acsuschemeng.5b01703>.
- G. Kuznetsov, V. Gerasimov, L. Sokolov, Sintering of polymeric powders under pressure - I. Ultrasonic analysis of the variation in contact between polymer powder particles, *Polym. Sci. U. S. S. R.* 6 (1964) 1391–1397, [https://doi.org/10.1016/0032-3950\(64\)90143-1](https://doi.org/10.1016/0032-3950(64)90143-1).
- W.W. Sampson, Materials properties of paper as influenced by its fibrous architecture, *Int. Mater. Rev.* 54 (2009) 134–156, <https://doi.org/10.1179/174328009X411154>.
- H. Fairbanks, Applying ultrasonics to the moulding of plastic powders, *Ultrasonics* 12 (1974) 22–24, [https://doi.org/10.1016/0041-624X\(74\)90082-1](https://doi.org/10.1016/0041-624X(74)90082-1).
- S. Matsuoaka, Effects of ultrasonic vibration on the compaction molding of polymeric powders, *J. Mater. Process. Technol.* 40 (1994) 443–450, [https://doi.org/10.1016/0924-0136\(94\)90467-7](https://doi.org/10.1016/0924-0136(94)90467-7).
- D. Paul, R. Crawford, Ultrasonic moulding of plastic powders, *Ultrasonics* 19 (1981) 23–27, [https://doi.org/10.1016/0041-624X\(81\)90028-7](https://doi.org/10.1016/0041-624X(81)90028-7).
- M.A. Beltran, D.M. Paganin, K. Uesugi, M.J. Kitchen, 2D and 3D X-ray phase retrieval of multi-material objects using a single defocus distance, *Opt. Express* 18 (2010) 6423–6436, <https://doi.org/10.1364/OE.18.006423>.
- D. Paganin, S.C. Mayo, T.E. Gureyev, P.R. Miller, S.W. Wilkins, Simultaneous phase and amplitude extraction from a single defocused image of a homogeneous object, *J. Microsc.* 206 (2002) 33–40, <https://doi.org/10.1046/j.1365-2818.2002.01010.x>.
- S. Dello, R. van Dam, J. Slangen, M. van de Poll, M. Bemelmans, J. Greve, R. Beets-Tan, Liver volumetry plug and play: do it yourself with ImageJ, *World J. Surg.* 31 (2007) 2215–2221, <https://doi.org/10.1007/s00268-007-9197-x>.
- N.W. Cheetham, L. Tao, Variation in crystalline type with amylose content in maize starch granules: an X-ray powder diffraction study, *Carbohydr. Polym.* 36 (1998) 277–284, [https://doi.org/10.1016/S0144-8617\(98\)00007-1](https://doi.org/10.1016/S0144-8617(98)00007-1).
- P. Tam Doo, R. Kerekes, Flexibility of wet pulp fibres, *Pulp Pap.* 83 (1982) 46–50.
- S. Gharekhani, E. Sadeghinezhada, S.N. Kazi, H. Yarmanda, A. Badarudina, M.R. Safaei, M.N.M. Zubir, Basic effects of pulp refining on fiber properties - a review, *Carbohydr. Polym.* 115 (2015) 785–803, <https://doi.org/10.1016/j.carbpol.2014.08.047>.
- T.-H. Le, P.J.J. Dumont, L. Orgéas, D. Favier, L. Salvo, E. Boller, X-ray phase contrast microtomography for the analysis of the fibrous microstructure of SMC composites, *Compos. Part A* 39 (2008) 91–103, <https://doi.org/10.1016/j.compositesa.2007.08.027>.
- S. Toll, Note: on the tube model for fiber suspensions, *J. Rheol.* 37 (1993) 123–125, <https://doi.org/10.1122/1.550460>.
- F. Martoia, P.J.J. Dumont, L. Orgéas, M.N. Belgacem, J.-L. Putaux, On the origins of the elasticity of cellulose nanofiber nanocomposites and nanopapers: a micro-mechanical approach, *RSC Adv.* 6 (2016) 47258–47271, <https://doi.org/10.1039/C6RA07176G>.
- C. Marulier, P.J.J. Dumont, L. Orgéas, S. Rolland du Roscoat, D. Caillerie, 3D analysis of paper microstructures at the scale of fibres and bonds, *Cellulose* 22 (2015) 1517–1539, <https://doi.org/10.1007/s10570-015-0610-6>.
- P.-J. Gustafsson, K. Niskanen, Paper as an engineering material, in: K. Niskanen (Ed.), *Mechanics of Paper Products*, De Gruyter, Berlin, 2012, pp. 5–26.
- T. Pintiaux, D. Viet, V. Vandenbosche, L. Rigal, A. Rouilly, Binderless materials obtained by thermo-compressive processing of lignocellulosic fibers: a comprehensive review, *BioResources* 10 (2015) 1915–1963.

- [31] J.C. Halpin, J.L. Kardos, Moduli of crystalline polymers employing composite theory, *J. Appl. Phys.* 43 (1972) 2235–2241, <https://doi.org/10.1063/1.1661482>.
- [32] S. Borodulina, A. Kulachenko, S. Galland, M. Nygård, Stress-strain curve of paper revisited, *Nord. Pulp Pap. Res. J.* 27 (2012) 318–328, <https://doi.org/10.3183/NPPRJ-2012-27-02-p318-328>.
- [33] H.L. Cox, The elasticity and strength of paper and other fibrous materials, *Br. J. Appl. Phys.* 3 (1952) 72–79, <https://doi.org/10.1088/0508-3443/3/3/302>.
- [34] M.F. Ashby, *Materials Selection in Mechanical Design*, 4 edition, Butterworth-Heinemann, Burlington, MA, 2010.
- [35] A. Regazzi, J. Viguié, B. Harthong, P.J.J. Dumont, et al., Ultrasonic welding of 100% lignocellulosic papers, *J. Mater. Sci.* 54 (19) (2019) 12938–12950, <https://doi.org/10.1007/s10853-019-03763-7>.